

000
001
002
003
004
005
006
007
008
009
010
011054
055
056
057
058
059
060
061
062
063
064
065
066
067
068
069
070
071
072
073
074
075
076
077
078
079
080
081
082
083
084
085
086
087
088
089
090
091
092
093
094
095
096
097
098
099
100
101
102
103
104
105
106
107

Partial Matching of 3D Shapes using Deformable Diversity

Anonymous CVPR submission

Paper ID ****

Abstract

We propose a novel approach for the matching of partial deformable shapes in 3D. Inspired by recent advances in 2D template matching techniques, our method relies on the concept of deformable diversity similarity(DDIS), extends and adapts it from an image to the 3D shape domain, and leverages the distinct behavior of this framework in different scales to achieve shape correspondences. We evaluate this framework on the SHREC16 partial matching of deformable shapes and show state of the art performance in achieving sparse correspondences. **Currently done Section 3 & 4**

1. Introduction

Shape correspondence is a fundamental and challenging problem in computer vision and graphics. It has usage in various applications such as transferring texture and animation. Shapes rarely, if ever manifest in only one pose. While rigid transformations between surfaces is a well researched topic with many adequate solutions, a more challenging problem arises when a shape is deformed non-rigidly, a case all too common for people, animals and objects. Moreover, the shape acquisition process almost always lead to partiality of the scanned object. Occlusions arise from different angles of acquisition, which cause an object to occlude itself, or stem from other occluding objects. An additional type of difficulty which might be occur is topological noise, occurring when shapes touch pn another, thus making sensors unable to seperate them. All of these combined give rise to the challenging problem of partial correspondences, where a deformed and incomplete shape, possibly with topological changes, has to be matched with its full version. The goal of this paper is to deal with this challenging problem.

While in a rigid setting the problem can be solved by RANSAC and ICP like approaches[25, 10], extending these to non-rigid case produces mediocre results due to an underlying assumption of small deformations. Early methods specialized for the non-rigid problem focused on minimiza-

tion of intrinsic metric distortion[6, 35] and regularity of parts[?, 4]. These methods all contain with them a global assumption of isometry which holds only approximately, these tended to break down with it, and are also unable to handle extreme partiality. Another family of method is based on functional correspondence. These methods model correspondences as a linear operator of a known nature between a space of functions on manifolds[19]. These methods, originally designed for the full shape correspondence scenario have achieved state of the art results on various partial matching tasks in the recent years[16, 36, 23], and produce dense correspondence maps, but are not parallelizable, and their reliance on intrinsic metrics makes them invariant to symmetry.

We take a different approach. We take advantage of the fact that while the isometric property tends to break over large distances, it usually holds approximately in limited environments. These also tend to suffer a lot less from boundary effects, especially when concentrated around the extremities of a shape.

We can thus treat the problem of partial correspondences as matching of multiple templates, each smaller then the partial surface centered around shape landmarks.

In addition, since point descriptors are known to be modified by partiality and deformations, instead of using them directly, we follow the approach of[33](**DDIS**) which tackles template matching in 2D and use simple statistical assumptions on the nature of nearest neighbors between small patch descriptors, along with the assumption of an approximate conservation of distances in medium environments to obtain similarity scores between these partial shape templates.

We analyze the behavior of DDIS similarity in different scales and devise a multi scale scheme which leverages the advantages of each scale while masking their shortcomings.

We show that using this approach, we are able to generate a set of sparse correspondences, which are less prone to symmetrical assignment than functional correspondence reliant methods, and are of superior quality on the SHREC16 Partial matching challenge[8]. We then demonstrate how these sparse correspondences can be used as an input to ex-

108
109
110
111
112
113
114
115
116
117
118
119
120
121
122
123
124
125
126
127
128
129
130
131
132
133
134
135
136
137
138
139
140
141
142
143
144
145
146
147
148
149
150
151
152
153
154
155
156
157
158
159
160
161
isting functional correspondence algorithms to obtain dense correspondences or a higher quality. In summary, our contributions are:

- A non trivial extension of Deformable Diversity from 2 to 3 Dimensions.
- A modified DDIS similarity measure which is more well suited to handle matching of templates with a different number of points.
- An empirical analysis of DDIS behavior in different scales, leading to an improved multi-scale framework.
- A multi-template approach to partial matching of deformable shapes which can both produce state of the art sparse correspondences, and be used as an input to functional correspondence algorithms, significantly improving the results obtained by these.

The rest of the work is organized as follows: in section 2 we go over related works in the field of shape analysis. Section 3 introduces our Deformable Diversity framework for 3D shape matching. Experiments and results are given in section 4, and the conclusions are in section 5.

2. Related work

2.1. Matching Of Deformable Surfaces

As a fundamental problem in computer graphics and vision, an extensive body of work have been done on the matching of surfaces. A variety of shape descriptors have been devised for this task which can be roughly divided in to 2 families. Extrinsic ones, such as PFH[26], SHOT[34] and FPFH[25] which are usually calculated in euclidean space and are thus sensitive to non rigid deformations, but can discern between reflections and are also more robust to noise, topological artifacts and boundary effects. On the other hand intrinsic features such as Heat[7] and Wave Kernel signatures[2] are invariant under isometric transformations, but are very sensitive to partiality and are unable to discern between symmetric parts. These have been commonly used to generate rough correspondences between surfaces and point clouds based on their similarity, but are noisy and offer little in terms of bijectivity and continuity of the solution. a measure of global consistency using these can be achieved by solving an energy minimization of the disimilarity matrices stemming from an assignment, and the auction algorithm has been commonly employed for this purpose. Other methods use pairwise relations between points such as geodesic distances[28, 29, 30], and search for a configuration which minimizes the distortions of these. These methods usually carry a high complexity, both due to calculating the pairwise relations, and the combinatorial configuration search, and are thus either obtain

sparse matches[28, 29, 30] to alleviate this complexity, or used strategies such as coarse to fine solutions. Another common approach has been to embed the shapes into a different lower dimension "canonical" space, this has been done by generalized MDS[6], an embedding into the mobius group[15], or by representation in the LBO basis[31] A notable family of works are derived from functional correspondences. Introduced at[19, 21, 13, 36] these assume that functions can be mapped from one manifold to another via a linear operator, finding this transfer operator allows to embed point in a space where the ICP method can obtain correspondences. Lately there has been a large body of works which employ learning methods such as Random Forests[22] and deep learning architectures[17, 3, 18]. These show the promise of achieving state of the art performance, but require a lot of annotated data.

2.2. Partial Matching of Deformable shapes

The introduction of partiality adds complications which are not present in the full correspondence scenario. Spectral quantities change drastically, while geodesic paths disappear. For the rigid setup, the Iterative Closest Point(ICP)[1] algorithm, preceded by initial alignment[27] tackle partial matching successfully. Adapting this to the rigid setup however has proved to have limited success due to the alignment which is necessary, and thus is only fit for very small non-rigid deformation.

Early works which were designed with partial matching in mind[4, 5] formulated an energy minimization problem over metric distortion and regularity of corresponding parts. Following works relaxed the regularity requirement by allowing for sparse correspondences[35, 24]. Other works[29, 28] minimized the distortion metric over the shape extremities by doing combinatorial search of least distortion matches and then densify them while employing a refining scheme in the process.

In[20] a bag of words point-wise descriptors on a part in conjunction with a constraint on area similarity and the regularity of the boundary length to produce correspondence less matching parts without point to point correspondences by energy minimization.

Another line of works employ machine learning techniques to learn correspondences between manifolds. Recently [23] had proven that partiality induces a slanted diagonal structure in the correspondence matrix and found the Laplacian eigenfunctions from each basis which induces this structure. Current state of the art[16] uses this notion in conjunction with joint diagnoilization. The main drawback of this method, shared with other intrinsic methods, is its invariance to symmetries.

3D Shape Descriptors

216 **2.3. Template matching in 2D**
217

218 Template matching in 2D is a well researched topic.
 219 Similarly to 3D objects are going complex deformations of
 220 pose, and are only seen partially depending on the camera
 221 point of view. Recently a series of works which use a very
 222 simplistic framework based on the statistical properties of
 223 nearest neighbors in low level feature space had made good
 224 strides in tackling this complex task.

225 **Best Buddies Similarity** Great strides had been
 226 achieved in the field of 2D template matching. Best Buddies
 227 Similarity[9] is a simple framework which employs
 228 a statistical assumption - if two regions \mathcal{N}, \mathcal{M} contain the
 229 same template patches should maintain Bi Directional Simi-
 230 larity. That is - given a point $n_i \in \mathcal{N}$ and a corresponding
 231 point $m_i \in \mathcal{M}$ they should point too each other as nearest
 232 neighbors - that is if $NN_{\mathcal{M}}(n_i) = m_j$ then on a matching
 233 template we should expect $NN_{\mathcal{N}}(m_j) = n_i$. Solving for a
 234 matching template then amounts to finding the region which
 235 has the highest count of best buddies. This amazingly sim-
 236 ple scheme has been show to be able to handle occlusions,
 237 missing parts and complex deformations of templates.

238 **Deformable Diversity Similarity** Building upon the
 239 above work, [33] relaxed the requirement for a best buddy
 240 relation, and added a requirement for spatial coherency.

241 The rather cumbersome best buddy relation has been re-
 242 laxled to requiring only that the diversity of the set of nearest
 243 neighbors sets between corresponding templates should be
 244 high. This is actually prerequisite to a high best buddies
 245 similarity score and serves as a rough approximation of it.
 246 For this end diversity is formally defined as:

$$247 \quad DIS = c \cdot |\{n_i \in \mathcal{N} : \exists m_j \in \mathcal{M}, NN(m_j, \mathcal{N}) = n_i\}| \quad (1)$$

248 where $|\cdot|$ denotes group size and $c = 1/\min(|\mathcal{M}|, |\mathcal{N}|)$ is
 249 a normalization factor. Between non corresponding win-
 250 dows, indeed one should expect most points to have no real
 251 corresponding point, and thus be mapped to a very and re-
 252 mote nearest neighbors. On the other hand, regions contain-
 253 ing matching objects are drawn from the same distribution,
 254 thus the diversity of nearest neighbors should be high. To
 255 accommodate this assumption not only did they rewarded
 256 high diversity of nearest neighbors, but also penalized map-
 257 ping to the same patch. To this end, another, a negative
 258 diversity measure had been defined:

$$259 \quad \kappa_{\mathcal{M}}(n_i) = |\{m \in \mathcal{M} : NN^a(m, \mathcal{N}) = n_i\}| \quad (2)$$

260 With x_i^a denoting the appearance descriptor of point x_i .
 261 Thus the contribution of a patch $m_j : NN^a(m_j, \mathcal{N}) = n_i$
 262 is $\exp(1 - \kappa_{\mathcal{M}}(n_i))$. An additional observation made has
 263 been that while non isometric deformations do occur, they
 264 should be restricted, small, in real objects. With distance
 265 on the window pixel grid between 2 nearest neighbor points

266 defined as $r_j = d(m_j^l, n_i^l)$ with x_i^l denoting the location
 267 of x_i on a grid, the final Deformable Diversity Similarity
 268 formulation becomes:

$$269 \quad DDIS = c \sum_{\mathcal{N} \rightarrow \mathcal{M}} \frac{1}{1 + r_j} \cdot \exp(1 - \kappa(NN^a(m_j, \mathcal{N}))) \quad (3)$$

270 **3. General Approach**
271

272 Given two surfaces \mathcal{M} and \mathcal{N} , the goal is to find the
 273 best match of \mathcal{N} within \mathcal{M} . In particular, we aim at ex-
 274 tracting a sparse set of point correspondences between the
 275 models. Our approach is based on three key ideas, which
 276 we describe hereafter.

277 First, inspired by [33], similarity is captured by two
 278 properties of the Nearest Neighbor field. (1) When \mathcal{N} and a
 279 patch of \mathcal{M} match, most points in \mathcal{M} have a unique NN-
 280 match in \mathcal{N} . This implies that the NN field should be
 281 highly diverse, in the sense that many different points in
 282 \mathcal{N} are being matched. (2) Arbitrary matches typically imply
 283 a large deformation, whereas correct matches should pre-
 284 serve the distance between pair of points. Therefore, Simi-
 285 larity should be based both on the diversity of the Nearest-
 286 Neighbor field and on the consistency of the distances be-
 287 tween the points.

288 Second, rather than realizing the similarity test, described
 289 above, on \mathcal{N} as a whole, it is preferable to perform it on a set
 290 of small sub-surfaces of \mathcal{N} . This is so not only since a small
 291 sub-surfaces is more likely to exhibit consistent distances,
 292 but also since it is less likely to be matched to a repeating
 293 pattern, which would lead to smaller diversity.

294 Third, a multi-scale approach with respect to the size of
 295 matched sub-surfaces is beneficial. This is so since larger
 296 surfaces contain more global context, resulting in matches
 297 which lie in a correct region, but provide poor localization.
 298 On the other hand, matching smaller surfaces lead to results
 299 which are better locally, but may be globally inconsistent.
 300 **AT: what do you mean by globally inconsistent?**

301 Therefore, our algorithm, which is illustrated in Figure 1,
 302 consists of the following steps.

- 303 **1. Pre-processing.** Shape descriptors are calculated for
 304 every vertex of both meshes and an approximate near-
 305 est neighbor field is computed for the vertices, as de-
 306 scribed hereafter.

307 Many descriptors have been proposed in the litera-
 308 ture [27, 34, 32]. We use the FPFH [25], which is ro-
 309 bust to small deformations and partiality of the data,
 310 yet sensitive to symmetrical flips. **AT: what makes**
 311 **it sensitive to symmetrical flips?** Therefore, it ad-
 312 dresses a major drawback of matching a right arm, for
 313 example, to the left one. We then compute a nearest
 314 neighbor field mapping, by assigning each vertex of
 315 \mathcal{M} its nearest neighbor in \mathcal{N} , FPFH-wise.

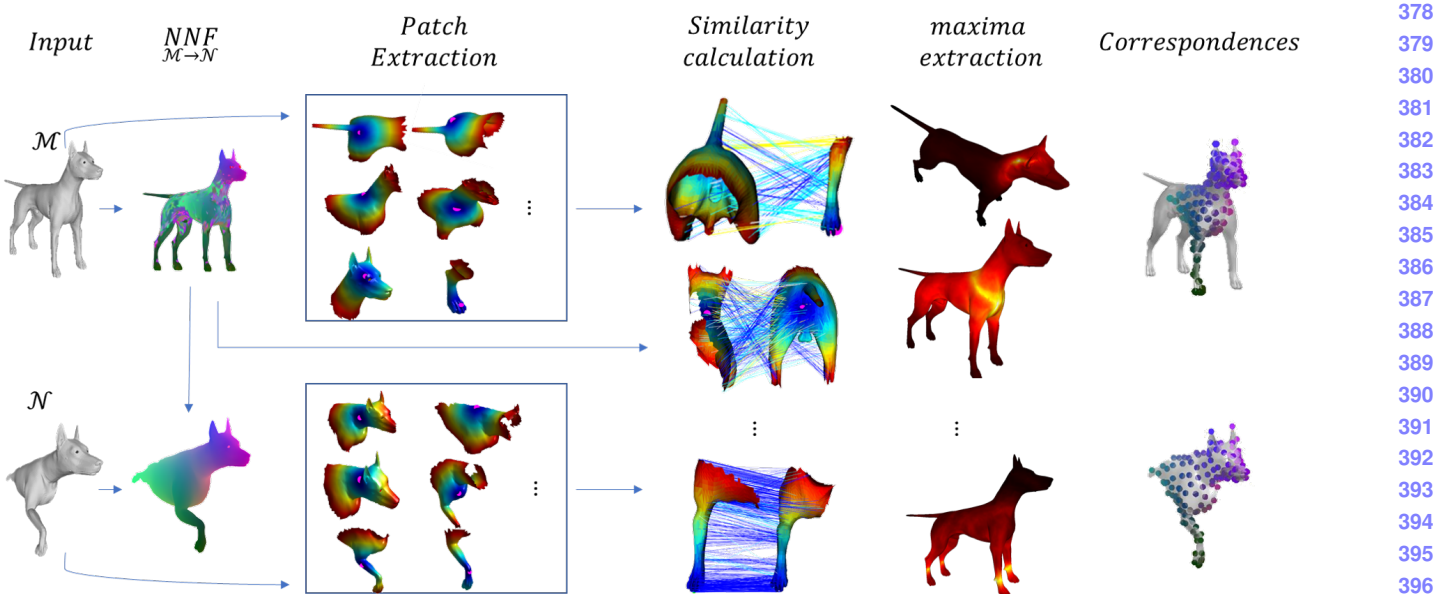


Figure 1. **Algorithm outline.** In the first step, we compute the nearest-neighbor field for \mathcal{N} and \mathcal{N} . Then, patches of the surfaces are extracted for every sample point in \mathcal{N} and for every vertex on \mathcal{M} . These patches cover the surface (i.e., may overlap) and represent semantic regions. Note that exact segmentation is not needed. Step 3 is the core of the algorithm, in which the similarity between the patches is computed. Finally, in Step 4, for every sample of \mathcal{N} we set the vertex of \mathcal{M} that achieves the maximal score as its corresponding point. **AT: This figure should be re-done**

2. Patch extraction. Inline with the second key idea, we aim at extracting a meaningful set of sub-surfaces, which cover (rather than partition) the surface. This is done in two steps: First, we extract a meaningful set of points, whose neighborhoods provide a good cover of the surface. We then extract the patches using this sample. We elaborate hereafter.

To extract the sample point set, we start from the extremities of the surface, which are considered salient points. A vertex is considered to be an extremity if it resides on a tip of the surface (e.g., tips of limbs) [11]. In practice, we define them to be vertices that are local maxima of the sum of the geodesic distance functional. Formally, $\forall v \in S$, let N_v be the set of neighboring vertices of vertex v . Let $GeoDist(v_i, v_j)$ be the geodesic distance between vertices v_i and v_j of mesh S . Vertex v is an extremity if it satisfies

$$\sum_{v_i \in S} GeoDist(v, v_i) > \sum_{v_n \in S} GeoDist(v_n, v). \quad (4)$$

Then, we iteratively add more samples, choosing the next sample point as follows. We construct a "forbidden" region around every point in the set. This region is a geodesic disc of radius $0.05\sqrt{Area(\mathcal{M})}$. The next point to be added to the set is a vertex whose geodesic distance to any sample point in the set is minimal and does not fall in any of the forbidden regions. This process stops when the entire surface is marked forbidden.

Once the set of representing sample set is defined, a disc (sub-surface) of geodesic distance R_T is extracted around each sample point, which is the sought-after set of patches. Specifically, $R_T = \beta \cdot \sqrt{Area(\mathcal{M})}$. As our approach is multiscale, β , which was found empirically by minimizing the error of correspondences on a training set, varies. In practice we use $\beta = \{0.6, 0.4, 0.2\}$.

3. Computing similarities between pairs of patches.

This step is the core of our algorithm, which realizes the first key idea.

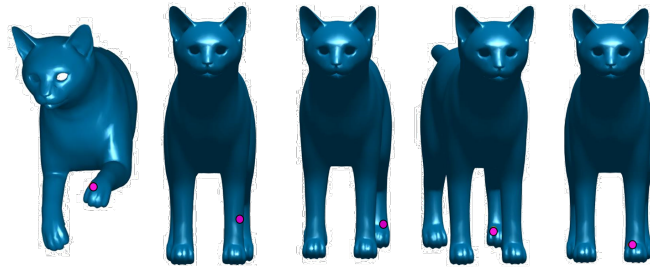
For each pair of patches of the same scale, $Q_i \subset \mathcal{M}$ and $P_i \subset \mathcal{N}$, we compute a similarity value. Recall that our goal is to reward a nearest-neighbor field with high diversity and low deformation. We will define the similarity function $DDIS$ that achieves it in Section 4. This is done in a multi-scale manner.

4. Extracting a sparse set of corresponding points.

Given the similarity values between the patches, our goal now is to extract a set of corresponding points between \mathcal{N} to \mathcal{M} . If we had a single scale, then for each sample point (the center of a patch) of \mathcal{N} , we would choose the vertex of \mathcal{M} that maximizes the similarity function.

In our multi-scale approach, we proceed from coarse to fine. Suppose that $P_i \subset \mathcal{N}$ and $Q_j \subset \mathcal{M}$ were

432 found to have the highest similarity in a coarsest scale
 433 (i.e. Q_j is the largest). The coarsest match is then
 434 set between $v_i \in P_i$ and $w_j \in Q_j$, where v_i, w_j are
 435 the *geodesic centers* of P_i, Q_j , respectively (i.e. the
 436 sample points that define the patches in Step 2). When
 437 moving to the finer scale, we replace Q_j with a smaller
 438 (finer) patch in which w_j is the center and set the new
 439 w_j to be the vertex on this patch that maximizes the
 440 similarity function $DDIS$ on this patch. The finest w_j
 441 is the corresponding point of v_i ; see Figure 2.
 442



443
 444 **Figure 2. Multi-scale similarity.** Given the sample point on the
 445 left (in magenta), the corresponding points on \mathcal{M} are shown on
 446 the right. In the coarsest level, the general region of the matching
 447 point is found, but the point is imprecise. In subsequent levels, the
 448 general region is not found. Our multi-scale approach manages to
 449 find the precise point. **AT: Replace the image. NA: done**

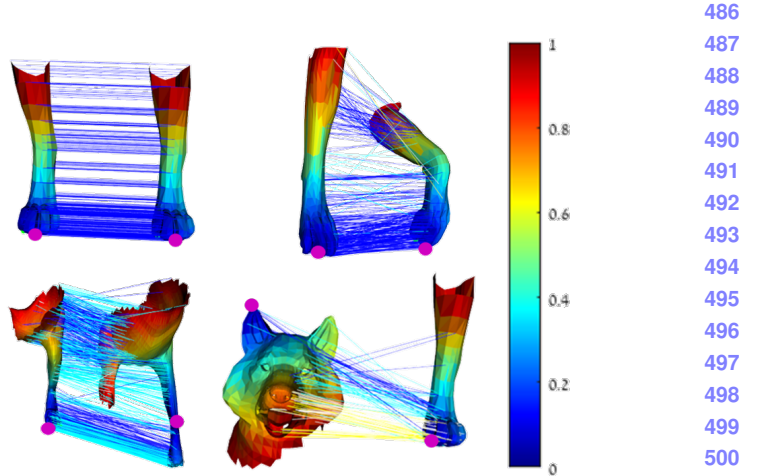
450
 451
 452
 453
 454
 455
 456
 457
 458
 459
 460 **5. Coherency-based correspondence refinement** The
 461 result of Step 4 is a set of corresponding pairs of points.
 462 In most cases ($> 92\%$ on all our examples), the corre-
 463 spondences are correct. The goal of this step is to iden-
 464 tify the incorrect ones and replace them by the correct
 465 correspondences.
 466

467 The key idea is to utilize coherency, i.e., if all points in
 468 the neighborhood of point $v \in \mathcal{N}$ are mapped to points
 469 that reside on the same region on \mathcal{M} , it is expected
 470 that the corresponding point of v , $w \in \mathcal{M}$, will also
 471 reside in this region. In other words, we are looking
 472 for outliers of the mapping.

473 To detect these outliers, we check the sum of geodesic
 474 distances. For a pair of points (v, w) to be considered
 475 correct, they should satisfy:

$$\sum_{v_i \in \mathcal{M}} |GeoDist(v, v_i) - GeoDist(w, w_i)| < C \quad (5)$$

477
 478 where w_i is the corresponding point of v_i and C is 0.15
 479 of the mean of Equation (5) on all points. We replace
 480 the corresponding point of an outlier by a point that
 481 minimizes Equation (5) and is a local maximum of the
 482 similarity function of Step 3.



483 **Figure 3. Nearest Neighbor Field.** The surfaces are colored by the
 484 geodesic distances from the magenta point; the lines are colored by the
 485 **NA: difference of geodesic distances from the purple point.**
 486 **AT: deviation of what?** Clearly, similar surfaces on the top (even
 487 when deformed) exhibit diversity in matching (i.e. different points
 488 on one surface are matched to different points on the other). Fur-
 489 thermore, in this case, most lines are blue, which indicates similar
 490 distances from the source point. This is not the case at the bottom,
 491 where the surfaces are highly different from one another.

4. Similarity

502 This section elaborates on Step 3, which is the core of the
 503 algorithm. Given pair of patches of the same scale, $Q \subset \mathcal{M}$
 504 and $P \subset \mathcal{N}$, this section defines a similarity function,
 505 termed *3D Deformable Diversity Similarity (3D-DDIS)*, be-
 506 tween them. This function should be oblivious to non-rigid
 507 transformation, different resolutions of the meshes, noise,
 508 and partiality of the data.

509 Recall that the key idea is to reward a point (center of
 510 the patch) whose nearest-neighbor field satisfied two prop-
 511 erties: it has both high diversity and low deformation. As
 512 for diversity, when Q and P correspond, most of the points
 513 on Q points have a unique NN-match on P . Conversely, if
 514 Q and P do not correspond, most of the points on Q do not
 515 have a good match on P , and therefore the nearest neigh-
 516 bors are likely to belong to a small set of points that happen
 517 to be somewhat similar to the points of Q . This implies that
 518 the NN-field is highly *diverse*, pointing to many different
 519 points in P . In addition, if two patches correspond, pairs
 520 matching (nearest neighbors) points tend to have similar
 521 geodesic distances to the centers of the patches they reside
 522 on. Conversely, arbitrary matches typically do not maintain
 523 such distances. **AT: why is it called deformation?**

524 To realize these requirements, we start by formally
 525 defining the diversity, $Div(Q, P)$, and the deformation,
 526 $Def(Q, P)$, and then show how to put them together into a
 527 similarity function. An intuitive and efficient way to mea-
 528 sure these properties is to consider the distribution of
 529 the geodesic distances from the centers of the patches to
 530 their nearest neighbors. The diversity is measured by
 531 the entropy of this distribution, while the deformation
 532 is measured by the standard deviation of the distances.
 533

534
 535
 536
 537
 538
 539

540 sure diversity is to count the number of unique NNs between
 541 the points of Q and P :

$$543 \quad Div(Q, P) = |\{p_i \in P : \exists q_j \in Q, NN(q_j, P) = p_i\}|, \quad (6)$$

544 where $\{p_i\}_{i=1}^{|P|}$ and $\{q_j\}_{j=1}^{|Q|}$ are the set of points of Q and P ,
 545 respectively and the nearest neighbors is computed between
 546 the descriptors (FPFH) of the points. However, we will see
 547 below that the diversity can be calculated implicitly.
 548

549 Next, we define $Def(Q, P)$, the deformation from Q to
 550 P . Let $p \in P$ and $q \in Q$ be the centers of P and Q , respec-
 551 tively; furthermore, let $p_i = NN(q_j, P)$ be the nearest-
 552 neighbor of $q_j \in Q$. The deformation implied by the NN-
 553 Field for p_i, q_j is defined by:
 554

$$555 \quad def(q_j, p_i, Q, P) = |GeodDist(q_j, q) - GeodDist(p_i, p)|, \quad (7)$$

556 where $0 < \epsilon \ll Area(\mathcal{M})$ and is used for numerical
 557 stability.
 558

559 For each $p_i \in P$, we find the minimal deformation
 560 $r_i^* = \min_{q_j \in Q} def(q_j, p_i, Q, P)$ such that p_i is the nearest
 561 neighbor of q_j . Note that some points in P might not be as-
 562 sociated with any point in Q (since they are not the nearest
 563 neighbors of any point $q_j \in Q$); in this case $r_i^* = \infty$.
 564

565 Having defined diversity between patches and deformation
 566 between points on these patches, we define the similarity
 567 between patches p and Q as:

$$568 \quad DDIS(P, Q) = \sum_{p_i \in P} \frac{1}{1 + r_i^*}. \quad (8)$$

569 It is easy to see how the 3D-DDIS rewards low deformation.
 570 However, we will explain hereafter why it also rewards
 571 high diversity. Consider a case where $r_i^* \in \{0, \infty\} \forall p_i$.
 572 When this occurs $\frac{1}{(1+r_i^*)} \in \{1, 0\}$ and it indicates that a
 573 point p_i has a point in Q that considers p_i to be its near-
 574 est neighbor. In this scenario, 3D-DDIS simply counts the
 575 number of points in Q that are nearest neighbors of some
 576 point in P . But, this is precisely the diversity function we
 577 seek-after. **AT: copy a convincing explanation for the**
 578 **general case** **NA: In the general case, the contribution**
 579 **of every point is inversely weighted by its deformation**
 580 **r_i^* , which gives preference to plausible deformations of**
 581 **real objects.**

585 5. Results

586 **AT: first paragraph: generally the datasets we ran**
 587 **on** **NA: We have evaluated our method both qualita-**
 588 **tively and quantitatively on the challenging bench-**
 589 **marks of SHREC 16 Partial Matching of Deformable**
 590 **Shapes[8]and SHREC'16: Matching of deformable**
 591 **shapes with topological noise[14], achieving results com-**
 592 **parable or better to state of the art on both.**

593 **Qualitative results:** xxx

594 **AT: second paragraph: qualitative results - images +**
 595 **comparisons + explanation** **NA: We provide a qualita-**
 596 **tive visual evaluation of our method along with a com-**
 597 **parison to the method with that of [23] in the case of the**
 598 **Partial Matching of Deformable Shapes dataset. It can**
 599 **be seen (in Fig 5) that our method can obtain sparse cor-**
 600 **respondences of a high quality, which can be then turned**
 601 **into dense ones with negligent loss of quality by feeding**
 602 **them to the method of [16] as delta functions. Our meth-**
 603 **ods explicit usage of distance preservation tends to result**
 604 **in more coherent solutions and mostly avoid symmetri-**
 605 **cal assignments, which plague [23]. The improvement is**
 606 **especially felt in the case of the holes dataset.**

607 **Quantitative results:** xxx **AT: next paragraphs: quan-**
 608 **titative results - explain the datasets in one paragraph,**
 609 **the error metrics in one paragraph, and explanations**
 610 **of the graphs+tables/results - one paragraph per graph**
 611 **NA: We provide quantitative evaluation of our method**
 612 **on both datasets w.r.t previously reported results on the**
 613 **benchmarks.**

614 **Error Metrics** **We evaluate correspondence quality**
 615 **according to the princeton benchmark protocol[12] de-**
 616 **tailed hereafter. Given a correspondence points** $(q, p) \in$
 617 **$\mathcal{N} \times \mathcal{M}$ produced by an algorithm, when the ground**
 618 **truth correspondence is** (q, p^*) . The error of the said
 619 **correspondence is measured by the normalized geodesic**
 620 **distance on** \mathcal{M} :

$$621 \quad \varepsilon(q) = \frac{GeoDist_{\mathcal{M}}(q, p^*)}{\sqrt{area(\mathcal{M})}} \quad (9)$$

622 **We plot cumulative curves showing the percentage of er-**
 623 **rors falling below a variable threshold. Symmetric solu-**
 624 **tions are accepted with no penalty. We report results**
 625 **both for the sparse correspondences produced by our**
 626 **algorithm, and dense ones, produced by feeding the for-**
 627 **mer to the method of [16].**

628 **Part to Full** **We have carried out a quantitative eval-**
 629 **uation of the partial matching scenario on the SHREC'16**
 630 **Partial Deformable Shapes benchmark. The benchmark**
 631 **contains 400 partial shapes, each a near isometrically**
 632 **deformed version of one of 8 base class. Each class is**
 633 **provided with a "null" shape in a neutral pose. The**
 634 **partial shapes are further divided into 2 subsets, deter-**
 635 **mined by the type of partiality. cuts, which is composed**
 636 **of shapes produced by dividing shapes by a plane, and**
 637 **holes, obtained by eroding many areas around random**
 638 **vertices. The size of the parts ranges from 800-9k ver-**
 639 **tices. We report our results in Figures 55. We compare**

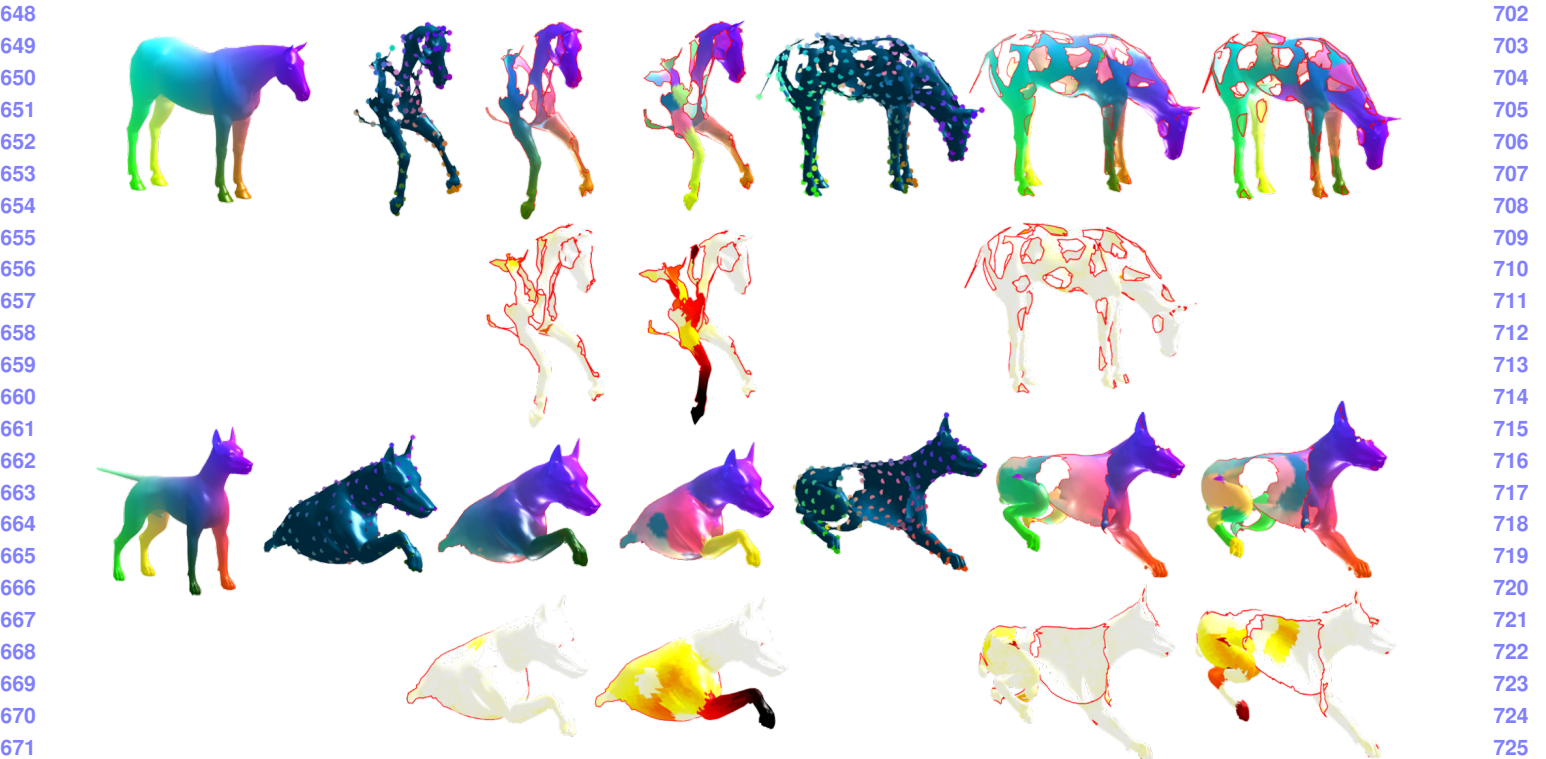
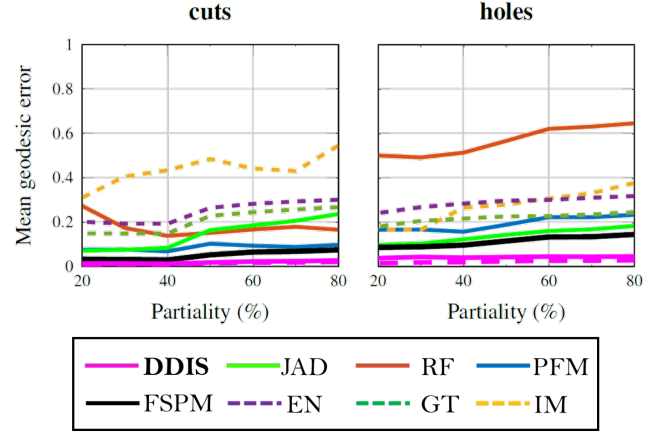
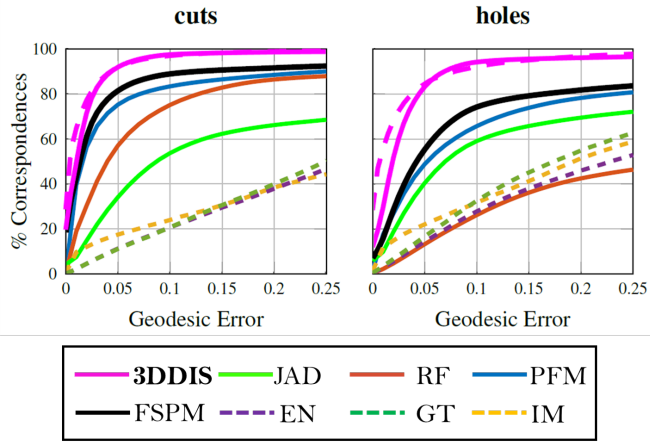


Figure 4. Results on Shrec'16 partial benchmark. in the right column we have the null shape. Each part triplet includes our sparse result, the dense correspondence extension, and the result obtained by PFM[23]. Below each dense correspondence we illustrate the geodesic error.



them with the results reported in Fully Spectral Partial Matching(FSPM)[16], which also compares results with partial functional maps(PFM)[23], random forests(RF), scale-invariant isometric matching(IM), game-theoretic matching(GT), elastic net matching(EN) and joint diagonalization. Methods producing sparse matches are marked in a dashed line, whereas full correspondences

are marked with a full line. We produced the graphs for our method using the code provided in the benchmark site. We can see from the plots that our method produces a considerable improvement over the previous state of the art method of FSPM. On the cuts dataset an improvement of 10% is seen while an impressive 20% is achieved over the holes dataset.

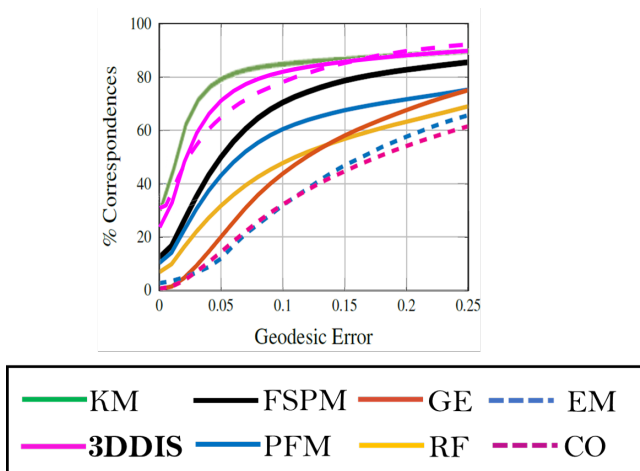


Figure 7. Error as a function of model partiality.

Topological changes We have also performed a quantitative evaluation on the SHREC 16 Topological noise benchmark[14]. The low resolution benchmark includes 10 shapes with 10K vertices each, derived from the same base human shape which undergoes deformations and topological changes stemming from self intersection. Each shape is matched to all the others resulting in 90 matching problems. We compare our results with those reported in[36] in Figure 5.

We can see from the plot that we fall short of achieving state of the art results on this benchmark. The additional paths between points introduced by topological noise causes significant problems in matching, especially around the noisy areas, a fact that[36] manages to tackle partially by optimizing over different distance kernels along with descriptor similarity. It might be worthwhile to find a way to incorporate these kernels into the 3D-DDIS framework.

Drawbacks: xxx AT: fifth paragraph: drawbacks with examples NA: Our method exhibits a few drawbacks. First and foremost is the asymptotic runtime - generating geodesic distances has an asymptotic complexity of $O(n^2 \log n)$ and computing 3D-DDIS similarity has an asymptotic runtime of $O(|S|n^2)$, which makes running on meshes with more than 15K vertices prohibitive. The algorithm also has six parameters which should be tuned. Additionally, surface patches such as the cat's tail, which are low in distinct shapes are hard to match. Finally, the method exhibits real difficulty dealing with topological noise.

Implementation details: xxx AT: sixth paragraph: implementation details, how do we move from sparse to dense NA: Our code which produces the sparse

correspondences is implemented entirely in C++ . For geodesics we have used Fast Marching Geodesics adapted from the code published by Ron Kimmel. FPFH is calculated using the Point Cloud library[] using a radius of $0.03\sqrt{M}$. Nearest Neighbor field is computed with FLANN[] with χ^2 distance. The entire code is parallelized using OpenMP. Since computing similarity for a given patch is totally independent from similarity calculations of all other patches the speedup is nearly linear in the number of threads. To move from sparse to dense correspondence we employ the method of [16], and replace the SHOT descriptors with localized smooth delta functions, effectively skipping straight to the refinement stage of that algorithm. It is also only necessary to run one iteration instead of 5 when using our correspondences to achieve superior quality of correspondences.

Alternatives: xxx AT: sixth paragraph: alternatives—comparison to Lihi's function, parameter tuning

Alternatives: xxx AT: seventh paragraph: uses in archaeology

5.1. Experimental Results

In this section we will briefly go over the available Datasets **SHREC 2016 Partial Correspondence** The SHREC partial matching dataset[8] consists of 8 base, neutral pose models: cat, centaur, dog, horse, wolf, and 3 humans – 2 males, and 1 female, each containing 10,000 vertices except for the wolf which contains only 4,500 vertices. Each basic model has corresponding deformed partial shapes obtained either by cutting the shape with a plane or by adding holes on a deformed shape. The set has been divided into train and test sets. The train set is composed of 15 cuts for each base models totaling 120 models, and 10 holed shapes for each model for which ground truth point to polygon correspondences has been provided in barycentric coordinates. The test set is composed of additional 200 cuts and 200 holed shapes. We have tuned our parameters only on the 120 pairs of cuts.

5.2. Error Metrics

The output of partial matching algorithms (as defined in[8]) are sub-vertex point-to-point correspondences between partial shapes. For all experiments we use the standard practice of not penalizing symmetric solutions. Quality is measured according to the Princeton benchmark protocol [12]. For a pair of points $(x, y) \in \mathcal{N} \times \mathcal{M}$ between the full object \mathcal{M} and the partial shape \mathcal{N} produced by an algorithm, where (x, y^*) is the ground truth correspondence the inaccuracy is measured by. We plot curves showing

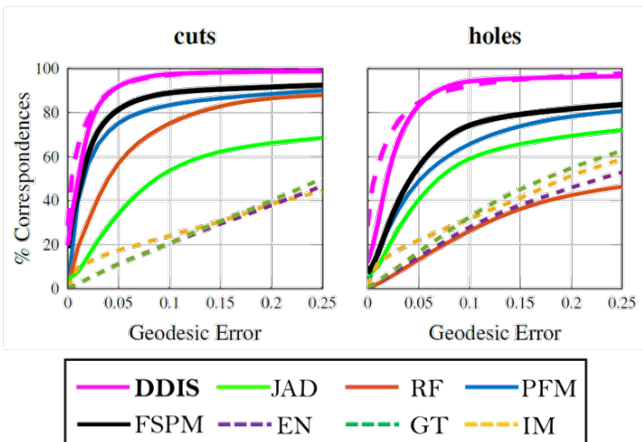


Figure 8. comparison with other state of the art algorithms - it can be seen that although sparse in nature, the correspondence obtained by DDIS are much more accurate than the other methods. A separate analysis has been done for correspondences which include boundary points, which tend to be more noisy, and internal points which are more sparse

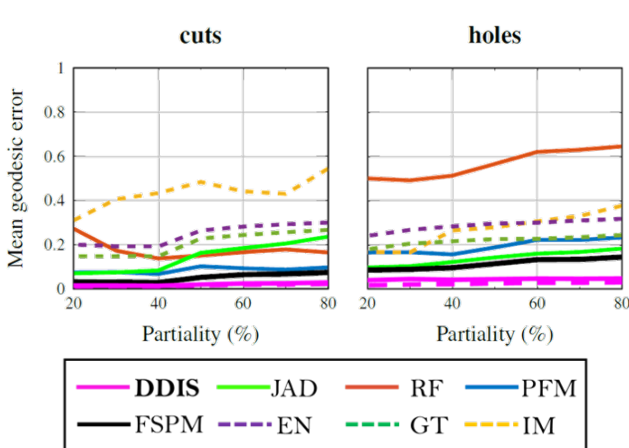
the fraction of correspondences whose errors are below a threshold of the normalized geodesic error

$$\varepsilon(x) = \frac{d_{\mathcal{M}}(y, y^*)}{\sqrt{\text{area}(\mathcal{M})}} \quad (10)$$

where $d_{\mathcal{M}}(y, y^*)$ is the geodesic distance on \mathcal{M} , and has units of normalized length on \mathcal{M} . For dense correspondences over a dataset, $\varepsilon(x)$ is averaged over all matching instances.

5.3. Sparse Correspondences on the SHREC16 Test set

We have tested the performance of DDIS in producing sparse correspondences on the SHREC16 Partial Matching of Deformable Shapes competition. We had tuned our parameters on the SHREC16 training dataset using only the cuts part of it. The best results had been produced using FPFH with $r_F = 0.03\sqrt{\text{Area}(\mathcal{M})}$, and a piece size radii of $R_T = [0.6, 0.4, 0.2]\sqrt{\text{Area}(\mathcal{M})}$. For Geodesic distances we have found the fast marching algorithm to work the fastest, while giving the lowest error w.r.t. to exact geodesics. For a 10,000 vertices mesh it takes 60s to produce a full distance matrix, Though it should be noted this algorithm has a more efficient GPU implementation, and parallelization on a core brought the run time to 12s with 6 threads. FPFH and Nearest Neighbor field takes 2s, and similarity between 2 pieces of 10000 vertices each takes 120s on average, running on 6 threads of i7-4790. Unlike optimization based algorithms this is highly parallelizable. We achieve results comparable to the state of the art [16] quality wise, even though sparser in nature on both the Cuts and the Holes datasets, Where a particularly impressive result is reported on the Holes dataset, which can then be expanded with a minimal loss of quality by feeding these to



[htb]

the FSPM[16] as input instead of low level shape descriptors.

	PFM	RF	IM	EN	GT	DDIS
cuts	dense	dense	61.3	87.8	51.0	132.2
holes	dense	dense	78.2	112.6	76.4	77.3

Table 1. mean number of correspondences obtained by the algorithms in the SHREC 16 competition and our algorithm. Note that our algorithm can combine wi

implementation Our code which produces the sparse correspondences is implemented entirely in C++ using the Point Cloud Library. For geodesics we have used Fast Marching Geodesics adapted from the code published by Ron Kimmel to run in parallel on multiple cores. We calculate FPFH using $R_{FPFH} = 0.03 \cdot \sqrt{\text{Area}(\mathcal{M})}$, and NNF using FLANN. The average runtime on i7-4790 for 2 surfaces of 12000 vertices is 150s.

References

- [1] D. Aiger, N. J. Mitra, and D. Cohen-Or. 4pointss congruent sets for robust pairwise surface registration. *ACM Trans. Graph.*, 27(3):85:1–85:10, Aug. 2008. 2
- [2] M. Aubry, U. Schlickewei, and D. Cremers. The wave kernel signature: A quantum mechanical approach to shape analysis. In *Computer Vision Workshops (ICCV Workshops), 2011 IEEE International Conference on*, pages 1626–1633. IEEE, 2011. 2
- [3] D. Boscaini, J. Masci, E. Rodolà, and M. Bronstein. Learning shape correspondence with anisotropic convolutional neural networks. In *Advances in Neural Information Processing Systems*, pages 3189–3197, 2016. 2
- [4] A. M. Bronstein and M. M. Bronstein. Not only size matters: regularized partial matching of nonrigid shapes. In

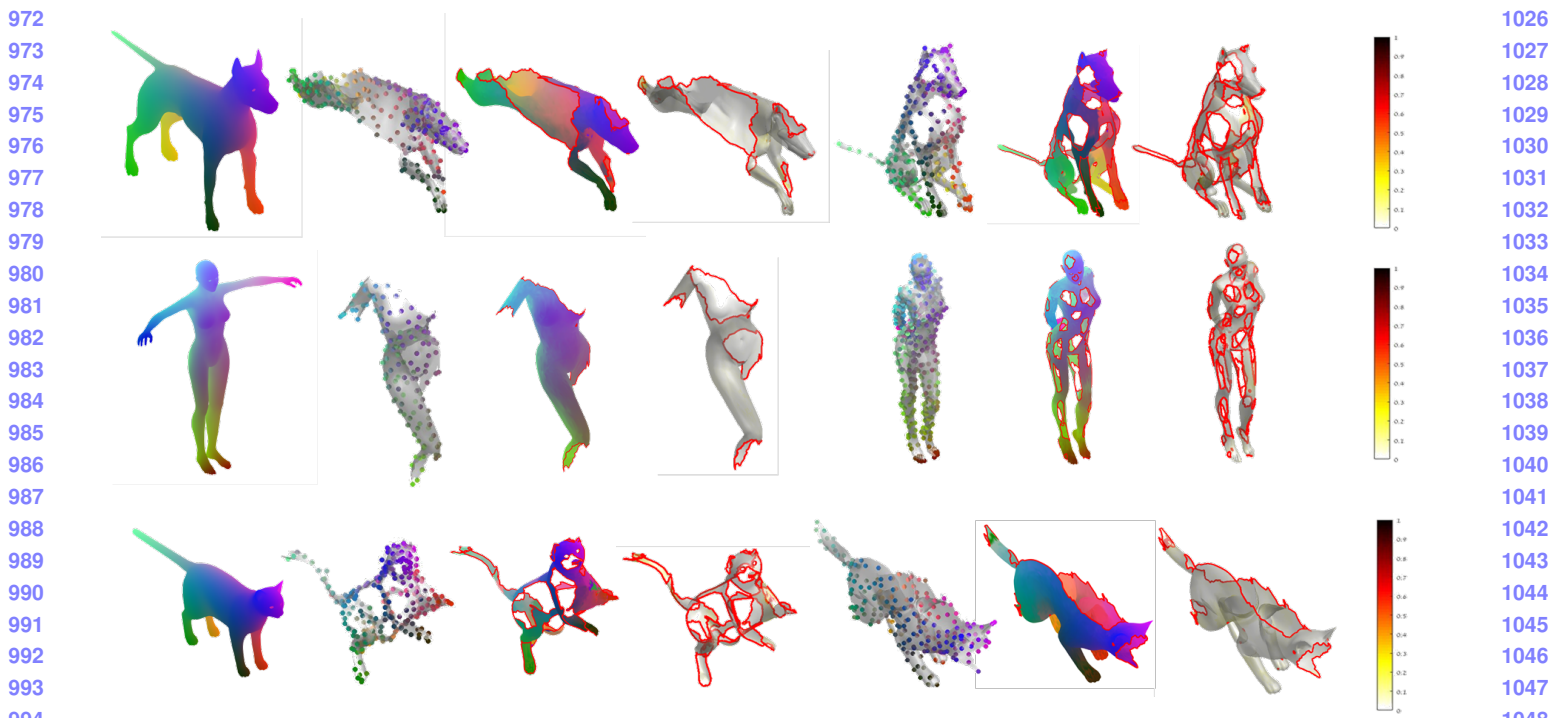


Figure 9. Good correspondences obtained by our method



Figure 10. Some notable failure cases

Computer Vision and Pattern Recognition Workshops, 2008. CVPRW'08. IEEE Computer Society Conference on, pages 1–6. IEEE, 2008. 1, 2

- [5] A. M. Bronstein, M. M. Bronstein, A. M. Bruckstein, and R. Kimmel. Partial similarity of objects, or how to compare a

centaur to a horse. *International Journal of Computer Vision*, 84(2):163, 2009. 2

- [6] A. M. Bronstein, M. M. Bronstein, and R. Kimmel. Generalized multidimensional scaling: a framework for isometry-invariant partial surface matching. *Proceedings of the Na-*

- tional Academy of Sciences, 103(5):1168–1172, 2006. 1, 2

[7] M. M. Bronstein and I. Kokkinos. Scale-invariant heat kernel signatures for non-rigid shape recognition. In *Computer Vision and Pattern Recognition (CVPR), 2010 IEEE Conference on*, pages 1704–1711. IEEE, 2010. 2

[8] L. Cosmo, E. Rodolà, M. Bronstein, A. Torsello, D. Cremers, and Y. Sahillioglu. Shrec’16: Partial matching of deformable shapes. *Proc. 3DOR*, 2, 2016. 1, 6, 8

[9] T. Dekel, S. Oron, M. Rubinstein, S. Avidan, and W. T. Freeman. Best-buddies similarity for robust template matching. In *Proceedings of the IEEE Conference on Computer Vision and Pattern Recognition*, pages 2021–2029, 2015. 3

[10] D. Holz, A. E. Ichim, F. Tombari, R. B. Rusu, and S. Behnke. Registration with the point cloud library: A modular framework for aligning in 3-d. *IEEE Robotics & Automation Magazine*, 22(4):110–124, 2015. 1

[11] S. Katz, G. Leifman, and A. Tal. Mesh segmentation using feature point and core extraction. *The Visual Computer*, 21(8-10):649–658, 2005. 4

[12] V. G. Kim, Y. Lipman, and T. Funkhouser. Blended intrinsic maps. In *ACM Transactions on Graphics (TOG)*, volume 30, page 79. ACM, 2011. 6, 8

[13] A. Kovnatsky, M. M. Bronstein, X. Bresson, and P. Vandergheynst. Functional correspondence by matrix completion. In *Proceedings of the IEEE conference on computer vision and pattern recognition*, pages 905–914, 2015. 2

[14] Z. Lähner, E. Rodolà, M. Bronstein, D. Cremers, O. Burghard, L. Cosmo, A. Dieckmann, R. Klein, and Y. Sahillioglu. Shrec’16: Matching of deformable shapes with topological noise. *Proc. 3DOR*, 2:11, 2016. 6, 8

[15] Y. Lipman and T. Funkhouser. Möbius voting for surface correspondence. *ACM Transactions on Graphics (TOG)*, 28(3):72, 2009. 2

[16] O. Litany, E. Rodolà, A. M. Bronstein, and M. M. Bronstein. Fully spectral partial shape matching. In *Computer Graphics Forum*, volume 36, pages 247–258. Wiley Online Library, 2017. 1, 2, 6, 7, 8, 9

[17] J. Masci, E. Rodolà, D. Boscaini, M. M. Bronstein, and H. Li. Geometric deep learning. In *SIGGRAPH ASIA 2016 Courses*, page 1. ACM, 2016. 2

[18] F. Monti, D. Boscaini, and J. Masci. Geometric deep learning on graphs and manifolds using mixture model cnns. 2

[19] M. Ovsjanikov, M. Ben-Chen, J. Solomon, A. Butscher, and L. Guibas. Functional maps: A flexible representation of maps between shapes. *ACM Trans. Graph.*, 31(4):30:1–30:11, July 2012. 1, 2

[20] J. Pokrass, A. M. Bronstein, and M. M. Bronstein. Partial shape matching without point-wise correspondence. *Numerical Mathematics: Theory, Methods and Applications*, 6(1):223–244, 2013. 2

[21] J. Pokrass, A. M. Bronstein, M. M. Bronstein, P. Sprechmann, and G. Sapiro. Sparse modeling of intrinsic correspondences. In *Computer Graphics Forum*, volume 32, pages 459–468. Wiley Online Library, 2013. 2

[22] E. Rodolà, S. R. Bulò, T. Windheuser, M. Vestner, and D. Cremers. Dense non-rigid shape correspondence using random forests. In *Proceedings of the 2014 IEEE Conference on Computer Vision and Pattern Recognition, CVPR ’14*, pages 4177–4184, Washington, DC, USA, 2014. IEEE Computer Society. 2

[23] E. Rodolà, L. Cosmo, M. M. Bronstein, A. Torsello, and D. Cremers. Partial functional correspondence. In *Computer Graphics Forum*, volume 36, pages 222–236. Wiley Online Library, 2017. 1, 2, 6, 7

[24] E. Rodola, A. Torsello, T. Harada, Y. Kuniyoshi, and D. Cremers. Elastic net constraints for shape matching. In *Proceedings of the IEEE International Conference on Computer Vision*, pages 1169–1176, 2013. 2

[25] R. B. Rusu, N. Blodow, and M. Beetz. Fast point feature histograms (fpfh) for 3d registration. In *Robotics and Automation, 2009. ICRA’09. IEEE International Conference on*, pages 3212–3217. Citeseer, 2009. 1, 2, 3

[26] R. B. Rusu, Z. C. Marton, N. Blodow, and M. Beetz. Learning informative point classes for the acquisition of object model maps. In *Control, Automation, Robotics and Vision, 2008. ICARCV 2008. 10th International Conference on*, pages 643–650. IEEE, 2008. 2

[27] R. B. Rusu, Z. C. Marton, N. Blodow, M. Dolha, and M. Beetz. Towards 3d point cloud based object maps for household environments. *Robotics and Autonomous Systems*, 56(11):927–941, 2008. 2, 3

[28] Y. Sahillioglu and Y. Yemez. Minimum-distortion isometric shape correspondence using em algorithm. *IEEE transactions on pattern analysis and machine intelligence*, 34(11):2203–2215, 2012. 2

[29] Y. Sahillioglu and Y. Yemez. Scale normalization for isometric shape matching. In *Computer Graphics Forum*, volume 31, pages 2233–2240. Wiley Online Library, 2012. 2

[30] Y. Sahillioglu and Y. Yemez. Coarse-to-fine combinatorial matching for dense isometric shape correspondence. In *Computer Graphics Forum*, volume 30, pages 1461–1470. Wiley Online Library, 2011. 2

[31] A. Shtern and R. Kimmel. Matching the lbo eigenspace of non-rigid shapes via high order statistics. *Axioms*, 3(3):300–319, 2014. 2

[32] J. Sun, M. Ovsjanikov, and L. Guibas. A concise and provably informative multi-scale signature based on heat diffusion. In *Proceedings of the Symposium on Geometry Processing, SGP ’09*, pages 1383–1392, Aire-la-Ville, Switzerland, Switzerland, 2009. Eurographics Association. 3

[33] I. Talmi, R. Mechrez, and L. Zelnik-Manor. Template matching with deformable diversity similarity. In *Proc. of IEEE Conf. on Computer Vision and Pattern Recognition*, pages 1311–1319, 2017. 1, 3

[34] F. Tombari, S. Salti, and L. Di Stefano. Unique signatures of histograms for local surface description. In *European conference on computer vision*, pages 356–369. Springer, 2010. 2, 3

[35] A. Torsello. A game-theoretic approach to deformable shape matching. In *Proceedings of the 2012 IEEE Conference on Computer Vision and Pattern Recognition (CVPR), CVPR ’12*, pages 182–189, Washington, DC, USA, 2012. IEEE Computer Society. 1, 2

1188	[36] M. Vestner, Z. Lähner, A. Boyarski, O. Litany, R. Slossberg,	1242
1189	T. Remez, E. Rodola, A. Bronstein, M. Bronstein, R. Kimmel, et al. Efficient deformable shape correspondence via	1243
1190	kernel matching. In <i>3D Vision (3DV), 2017 International Conference on</i> , pages 517–526. IEEE, 2017.	1244
1191	1, 2, 8	1245
1192		1246
1193		1247
1194		1248
1195		1249
1196		1250
1197		1251
1198		1252
1199		1253
1200		1254
1201		1255
1202		1256
1203		1257
1204		1258
1205		1259
1206		1260
1207		1261
1208		1262
1209		1263
1210		1264
1211		1265
1212		1266
1213		1267
1214		1268
1215		1269
1216		1270
1217		1271
1218		1272
1219		1273
1220		1274
1221		1275
1222		1276
1223		1277
1224		1278
1225		1279
1226		1280
1227		1281
1228		1282
1229		1283
1230		1284
1231		1285
1232		1286
1233		1287
1234		1288
1235		1289
1236		1290
1237		1291
1238		1292
1239		1293
1240		1294
1241		1295